Quantum Tunneling in the Midrange Vibrational Fundamentals of Tropolone

Richard L. Redington* and Theresa E. Redington

Department of Chemistry and Biochemistry, Texas Tech University, Lubbock, Texas 79409

Robert L. Sams

Wiley Environmental Molecular Sciences Laboratory, Pacific Northwest National Laboratory, Richland, Washington 99352

Received: April 3, 2006; In Final Form: May 25, 2006

The Fourier transform infrared spectrum of tropolone(OH) vapor in the 1175−1700 cm^{-1} region is reported at 0.0025 and 0.10 cm^{-1} spectral resolutions. The 12 vibrational fundamentals in this region of rapidly rising vibrational state density are dominated by mixtures of the CC, CO, CCH, and COH internal coordinates. Estimates based on the measurement of sharp Q branch peaks are reported for 11 of the spectral doublet component separations $DS_v = |\Delta_v \pm \Delta_0|$. $\Delta_0 = 0.974$ cm^{-1} is the known zero-point splitting, and three a_1 modes show tunneling splittings $\Delta_v \approx \Delta_0$, four b_2 modes show splittings $\Delta_v \approx 0.90\Delta_0$, and the remaining four modes show splittings Δ_v falling 5−14% from Δ_0. Significantly, the splitting for the nominal COH bending mode ν_8 (a_1) is small, that is, 10% from Δ_0. Many of the vibrational excited states demonstrate strong anharmonic behavior, but there are only mild perturbations on the tautomerization mechanism driving Δ_0. The data suggest, especially for the higher frequency a_1 fundamentals, the onset of selective intramolecular vibrational energy redistribution processes that are fast on the time scale of the tautomerization process. These appear to delocalize and smooth out the topographical modifications of the zero-point potential energy surface that are anticipated to follow absorption of the ν_v photon. Further, the spectra show the propensity for the Δ_v splittings of b_2 and other complex vibrations to be damped relative to Δ_0.

I. Introduction

Evidence for quantum mechanical tunneling by electrons, protons, and heavier entities has been available for many years, cf. the recent monograph *Quantum Theory of Tunneling* by Razavy,[1] and experimental data demonstrating details of various tunneling processes by C, N, O, and other heavy atoms is accumulating.[2] As suggested in Figure 1, the interconversions between energetically equivalent tautomers of tropolone (Tp), and of malonaldehyde (MA), are inherently multidimensional. This is because the OH···O → O···HO transfer also necessarily includes displacements of the heavy skeletal atoms. State-specific spectral doublets due to quantum tunneling have been reported for gaseous MA[3−13] and for gaseous and Ne-isolated Tp.[14−31] The spectral data provide, along with theoretical−computational results briefly noted below, compelling arguments for the multidimensional nature of the molecular tunneling mechanisms. The studies reported for MA and Tp position these substances as prototypes for the study of tunneling dynamics in molecules with 10 or 15 atoms and an intramolecular H-bond. Both substances host persistent experimental and theoretical−computational challenges.

In the S_0 electronic ground state, the zero-point (ZP) tunneling splitting observed for MA(OH)[8,9] (9 atoms with 6-atom H-bonded ring) is $\Delta_0 = 21.583$ cm^{-1}. The value for Tp(OH)[24] (15 atoms with 5-atom H-bonded ring) is $\Delta_0 = 0.974$ cm^{-1}. Similar precision has not yet been reached for the vibrational excited-state tunneling splittings Δ_v in the S_0 electronic ground state. With relatively few atoms, MA is a favored target for increasingly powerful theoretical treatments aimed at multi-dimensional tunneling processes in the ZP state and in excited vibrational states.[32−50] Tunneling splitting computations spanning the full 21 dimension vibration coordinate space of MA have been made,[32−35] and there has been significant progress on the multidimensional tunneling dynamics of Tp.[51−59] The steady advances of theoretical−computational methods concomitantly escalate the need for comparative experimental observations.

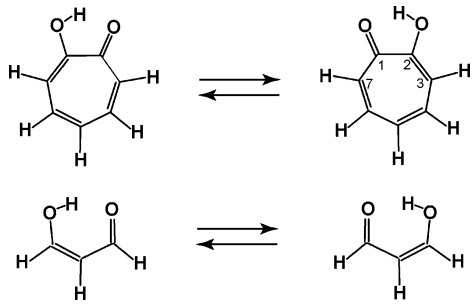

Figure 1. Energetically equivalent structures of tropolone (upper) and malonaldehyde (lower). Tautomerization occurs via multidimensional quantum tunneling processes through vibrational state-specific energy barriers.

II. Midrange Fourier Transform Infrared Spectrum of Tropolone Vapor

A. General Background. Figure 2 presents an overview of the Fourier transform infrared (FTIR) absorption spectrum of gaseous Tp(OH) in the 1175−1700 cm^{-1} region at 0.0025 cm^{-1} spectral resolution (25 °C, ca. 0.01 Torr sublimation pressure, and 32 m absorption path length). Origins for cold bands observed[16,26] in the IR spectrum of Ne-isolated Tp(OH) at ∼5 K are included along the abscissa as an aid for the spectral interpretation.

10.1021/jp062068s CCC: $33.50
Published on Web 07/18/2006

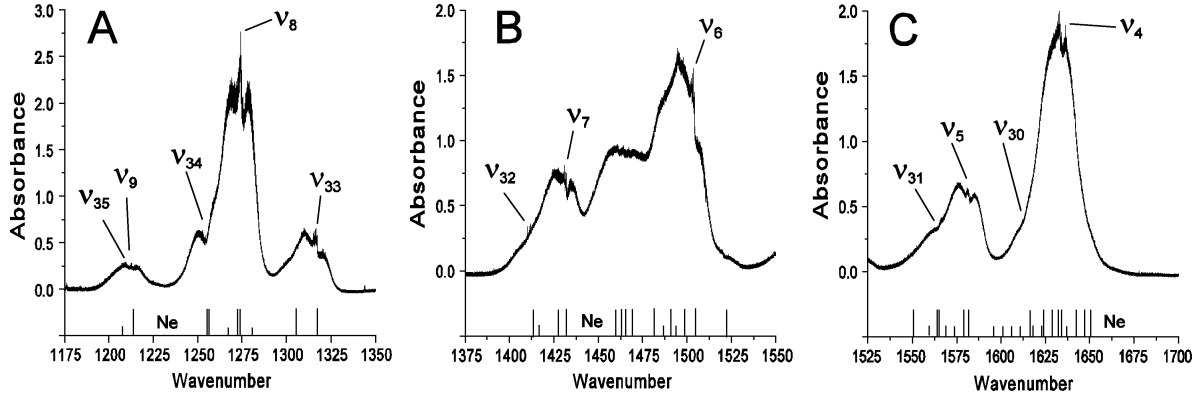

Figure 2. Overview of the Fourier transform infrared absorption spectrum for Tp(OH) vapor at 25 °C obtained at 0.0025 cm^{-1} spectral resolution. Origins for the transitions observed for Ne-isolated samples[16,26] at ~5 K by medium-resolution grating spectroscopy are shown along the abscissa. The shorter strokes locate minor peaks. (A) 1175−1350 cm^{-1} region; details in Figures 5−8. (B) 1375−1550 cm^{-1} region; details in Figures 9 and 10. (C) 1525−1700 cm^{-1} region; details in Figures 11 and 12.

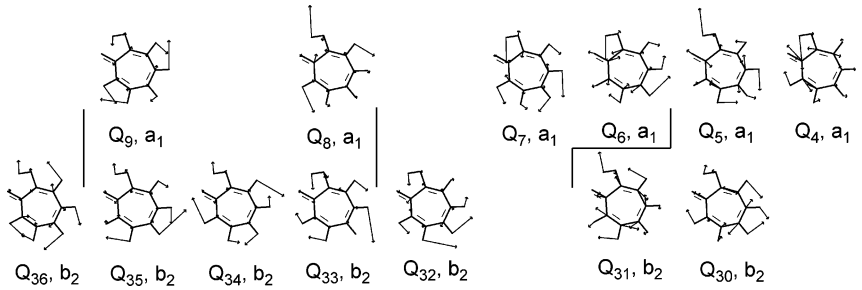

Figure 3. MO-computed[26] (harmonic) normal modes Q_υ, separated into a_1 and b_2 classifications (G_4 molecular symmetry group). Frequencies ω_υ increase as $\omega_{36} < \omega_9 < \omega_{35} < \omega_{34} < \omega_8$... (cf. Tables 1 and 2). Dividers separate the 13 modes as ν_{36} (not studied) | 5 modes in Figure 2A | 3 modes in Figure 2B | 4 modes in Figure 2C.

The overall IR spectrum of Tp shows many effects reflecting the multidimensional anharmonicity present in its basic double minimum potential energy surface (PES). Figure 3 shows the *harmonic* normal coordinates Q_υ computed[26,57] by use of a relatively high level of quantum chemistry theory designated here as MP2/GEN.[60] They reflect the behaviors of in-plane fundamentals composed of mixed COH bend, CH rock, CO stretch, and CC stretch internal coordinates. Their forms are sensitive[26,61] to both the basis set utilized and the correlation energy approximation, and they suggest transition dipoles with components lying on both the *Z* (longitudinal−fictive C_2) and the *Y* (transverse) axes. The present FTIR spectra clearly show evidence, through sharp Q spikes, for hybrid IR absorption profiles as illustrated in Figure 4 for the b_2 fundamentals.

The two lower levels in Figure 4 are separated by the ZP tunneling splitting Δ_0. Quantum numbers for the ZP steps of the contortional energy ladder[62] are $N_{con} = 0$ and $N_{con} = 1$, and the vibrational quantum numbers are $N_\upsilon = 0$ for all fundamental vibrations ($\upsilon = 1-39$). The upper levels are the lowest tunneling split contortion−vibration states determined by the equal double-minimum effective PES incorporating the excited-state vibrational energy. For a_1 vibrations (e.g., ν_8) the *Z*-polarized doublet transition components are expected to dominate over the *Y*-polarized transition components, with the opposite behavior anticipated for b_2 vibrations (e.g., ν_{34}).

Computations[63] of model IR absorption profiles for Tp at 25 °C show the *Z*-polarized transition dipole component produces a type A rotational contour characterized by a sharp central Q branch spike near the band origin. The P and R branch maxima are separated by about 7 cm^{-1}. The sharp central Q spike provides a reasonable estimate for the type A band origin, and the separation between Q spikes observed for the two type A components of a spectral doublet provides a reasonable first estimate for the doublet separation (DS_υ). This simple measurement avoids formidable rotational analyses of the many overlapping transitions found in the IR spectrum of gaseous Tp at room temperature. Figure 4 shows small DS_υ values occur for the putatively intense *Z*-polarized transitions of a_1 fundamentals ($DS_\upsilon = |\Delta_\upsilon - \Delta_0|$), with large DS_υ values for the putatively weak *Z*-polarized transitions of b_2 fundamentals ($DS_\upsilon = \Delta_\upsilon + \Delta_0$). The origin for a type B (*Y*-polarized) rotational contour[63] for Tp is near the central absorbance dip, and there is no sharp central Q branch spike.

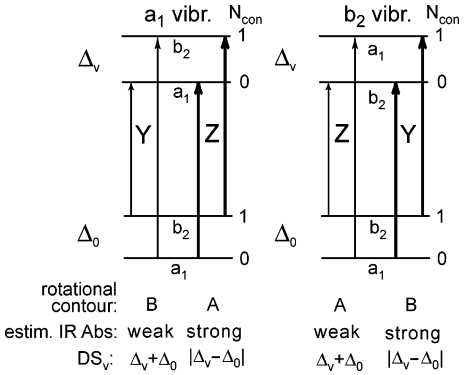

Figure 4. Schematic showing the spectral tunneling doublets arising from *Y*- (transverse) and *Z*- (longitudinal) polarized transition dipole components for the in-plane a_1 and b_2 vibrations of Tp. Δ_υ and Δ_0 are tunneling splittings in the excited vibrational state ν_υ and in the zero-point state, respectively. N_{con} are quantum numbers for the tunneling split contortional states. Type A and type B rotational contours possess and lack, respectively, sharp Q branch spikes marking the approximate band origins. DS_υ are separations of the spectral doublet components expressed in terms of the upper (Δ_υ) and lower (Δ_0) state tunneling splittings.

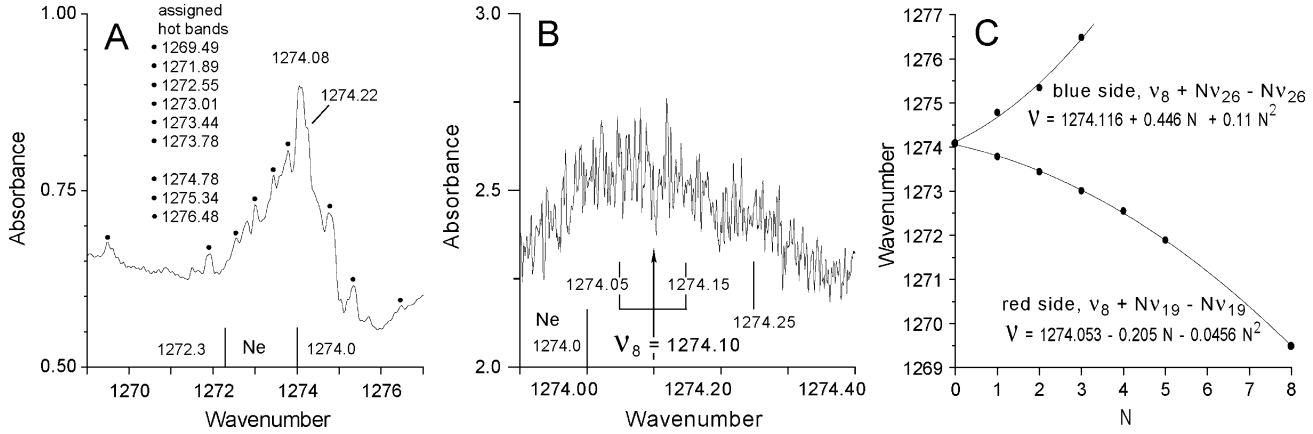

Figure 5. FTIR data in the central Q branch region of ν_8 (a_1), the nominal COH bending fundamental of Tp(OH). (A) Overview at 0.10 cm^{-1} resolution. Least-squares fittings of peaks (marked ●) to quadratic equations appear in panel C. (B) Tip region of the major spike at 0.0025 cm^{-1} resolution, showing estimated absorbance maxima at 1274.05 and 1274.15 cm^{-1} yielding ν_8 (a_1) = 1274.10 cm^{-1} and DS_8 = 0.10 cm^{-1}. (C) Least-squares fittings of points ● attributed to the unresolved hot band doublet peaks in panel A.

TABLE 1: Frequencies and Tunneling Splittings: a_1 Fundamentals

v	ν_v (cm^{-1})	DS_v (cm^{-1})	Δ_v (cm^{-1})	%[a]	ω_v[b] (cm^{-1})	Abs (km mol^{-1})
9	1212.59	0.14	1.11 or 0.83	14	1238	2
8	1274.10	0.10	1.07 or 0.87	10	1348	131
7	1431.27	≤0.14	≤1.11 or ≥0.83	≤14	1482	216
6	1502.53	0.00	0.97	0	1530	162
5	1582.88	0.00	0.97	0	1629	57
4	1634.09	0.00	0.97	0	1715	129

[a] $100|\Delta_v - \Delta_0|/\Delta_0$. [b] Unscaled ω_v values (refs 26 and 57). The ν_v/ω_v values range from 0.95 to 0.98.

B. Tunneling Doubling in the ν_8 (a_1) Nominal COH Bending Fundamental. The nominal COH bending fundamental ν_8 (a_1) of Tp(OH) dominates Figure 2A and, indeed, all of Figure 2. Since the ν_8 vibration involves significant motion by the transfer H atom, normal intuition would suggest that the excitation of ν_8 should strongly influence the tunneling mechanism and cause Δ_8 to differ appreciably from Δ_0 with the generation of an easily resolved DS_8 value. On the scale of Figure 2A, however, there is a single PQR absorption envelope for ν_8 (a_1) with no indication of wide spectral doubling.

Figure 5A shows the structured central Q branch spike region of ν_8 (a_1) at 0.1 cm^{-1} resolution, with the tip of the Q spike and adjacent shoulder shown at 0.0025 cm^{-1} resolution in Figure 5B. The structured profile suggests an underlying doublet through average apparent absorbance maxima near 1274.05 and 1274.15 cm^{-1}, and these values are chosen (with overrated precisions) to approximate DS_8. As entered in Table 1, these yield ν_8 (a_1) = 1274.10 cm^{-1}, $DS_8 = |\Delta_8 - \Delta_0| = 0.10$ cm^{-1}, and alternative choices $\Delta_8 = 1.07$ and $\Delta_8 = 0.87$ cm^{-1} for the tunneling splitting in the ν_8 (a_1) vibrational state. As noted in section III, evidence can be cited for both choices. (Using 1274.10 and the 1274.25 cm^{-1} shoulder for the ν_8 doublet would yield $\Delta_8 = 1.12$ or 0.82 cm^{-1}.) There is no apparent evidence to distinguish the weak *Y*-polarized doublet component in the ν_8 (a_1) absorption profile. In contrast, five of the six b_2 fundamentals show weak type A (*Z*-polarized) Q branch spike doublets with component separations $DS_v = \Delta_v + \Delta_0$ marking their hybrid absorption profiles.

The IR spectrum of Tp(OH) isolated in a Ne matrix[16,26] at ~5 K shows transitions at 1272.3 and 1274.0 cm^{-1} (Figures 2 and 5). These, and similar spectral "doublets" observed for the Ne-isolated OH/OD isotopomers, are due to separate trapping sites rather than to tunneling doubling.[64,65] The copious spectral structure seen in Figure 5A for gaseous Tp(OH) is not due to resolved tunneling transitions. It is systematically assigned to the linear/quadratic hot band progressions $\nu_8 + N\nu_{19} - N\nu_{19}$ with $N = 1-8$ to the red of ν_8 and $\nu_8 + N\nu_{26} - N\nu_{26}$ with $N = 1-3$ to the blue of ν_8 as illustrated in Figure 5C. The ν_{19} (a_2, 110 cm^{-1}, OCCO/skeletal twist) and ν_{26} (b_1, 177 cm^{-1}, OCCO/skeletal wag) modes are the lowest frequency fundamentals of Tp(OH) and they generate ubiquitous hot bands in the IR spectrum of tropolone.[26,27,31]

Tunneling doublets for the individual ν_8 (a_1) hot band Q spikes are not resolved at 0.10 cm^{-1} spectral resolution because the contortion−vibration selection rules for the hot band transitions yield $DS_{hot,N} = |\Delta_{N'} - \Delta_{N''}|$ (just as $DS_8 = |\Delta_8 - \Delta_0|$). The $\Delta_{N'}$ (upper) and $\Delta_{N''}$ (lower) splitting values are strongly damped relative to Δ_8 and Δ_0, respectively, to reduce the $|\Delta_{N'} - \Delta_{N''}|$ value relative to $|\Delta_8 - \Delta_0| = 0.10$ cm^{-1}. The strong damping of the $\Delta_{N'}$ and $\Delta_{N''}$ states is clearly seen for the b_2 fundamentals discussed below because for these $DS_{hot,N} = \Delta_{N'} + \Delta_{N''}$ (just as $DS_v = \Delta_v + \Delta_0$).

The complex IR absorption profile for Tp(OH) vapor at 25 °C seen in Figures 2 and 5 reduces to the simple 1272.3, 1274.0 cm^{-1} trapping site doublet under low-temperature Ne matrix isolation conditions and to a single peak at 1269.5 cm^{-1} in Ar.[26] With ν_8 (a_1) = 1274.10 cm^{-1} observed for the gas phase, the Ne- and Ar-induced vibrational frequency shifts are to the red at −0.9 and −4.6 cm^{-1}, respectively.

C. Tunneling Doubling in the Mixed-Mode CH Rocking Fundamentals of Figure 2A. The FTIR spectrum of Tp(OH) in the midrange region includes distinctive features including resolved spectral tunneling doublets, overtone−combination transitions, and intramolecular resonance couplings—with pronounced intermolecular interactions.

1. ν_{34} (b_2) = 1254.52 cm^{-1}. Figure 2A shows the ν_{34} (b_2) fundamental of Tp(OH) has a characteristic type B profile, and the detailed scans in Figure 6 show additional weak spikes at 1253.52 (vvw), 1253.99, 1254.62, and 1255.51 (vw) cm^{-1}. Tp(OH) isolated in solid Ne shows peaks at 1255.3 and 1256.2 cm^{-1} attributed to a site doublet,[65] and in solid Ar it shows a single peak at 1252.8 cm^{-1}.[26] The weak type A (*Z*-polarized) Q branch spikes of ν_{34} (b_2), separated by $DS_{34} = \Delta_{34} + \Delta_0 \approx 2$ cm^{-1}, are distinguished and assigned in Figure 6B. $DS_{34} = 1.99$ cm^{-1} yields $\Delta_{34} = 1.02$ cm^{-1}—5% larger than Δ_0—as entered in Table 2. The two intense peaks in Figure 6B are readily assignable as the Q spike doublet for the *Z*-polarized hot band $\nu_{34} + \nu_{19} - \nu_{19}$ to yield $DS_{hot} = \Delta' + \Delta'' = 0.63$

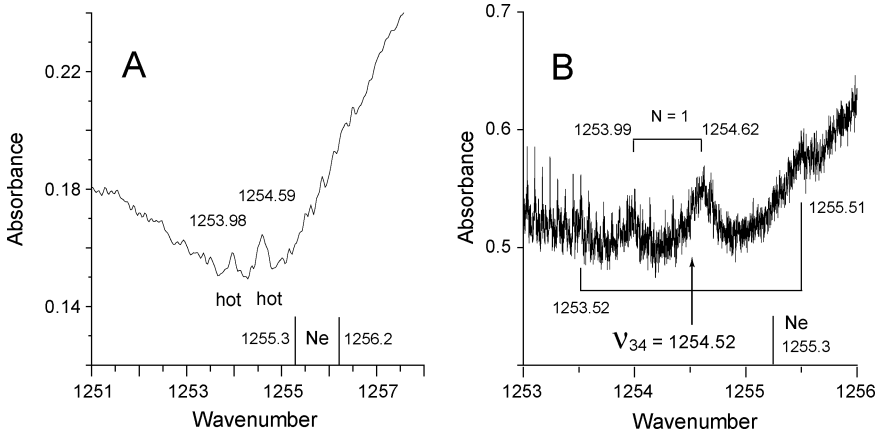

Figure 6. (A) FTIR data for the ν_{34} (b_2) origin region at 0.10 cm^{-1} resolution. (B) Spectrum at 0.0025 cm^{-1} resolution with assignments given for the weak type A (*Z*-polarized) Q spikes yielding the vibrational frequency ν_{34} (b_2) = 1254.52 cm^{-1}. The more intense peaks are for the corresponding Q spikes of the weak $\nu_{34} + \nu_{19} - \nu_{19}$ ($N = 1$) hot band doublet.

TABLE 2: Frequencies and Tunneling Splittings: b_2 Fundamentals

v	ν_v (cm^{-1})	DS_v (cm^{-1})	Δ_v (cm^{-1})	%[a]	ω_v[b] (cm^{-1})	Abs (km mol^{-1})
36	(1051)[c]				1083	1
35	1208.43	1.86	0.89	−8	1247	3
34	1254.52	1.99	1.02	+5	1280	23
33	1315.21	1.86	0.89	−8	1370	46
32	1411.94	1.85	0.88	−9	1450	1
31	1565.57	1.85	0.88	−9	1585	153
30	1616.0	not obs			1653	15

[a] 100 $|\Delta_v - \Delta_0|/\Delta_0$. [b] Unscaled ω_v values (refs 26 and 57). The ν_v/ω_v values range from 0.96 to 0.99. [c] Reference 26. ν_{36} was not studied in the present work.

cm^{-1}. This value is greatly reduced from DS_{34} to demonstrate that $\Delta'(\nu_{34} + \nu_{19})$ and $\Delta''(\nu_{19})$ are strongly damped relative to Δ_{34} and Δ_0. Damping of the Δ_{19}, $\Delta_{2\nu_{19}}$, $\Delta_{3\nu_{19}}$, and $\Delta_{4\nu_{19}}$ states relative to Δ_0 has been previously noted.[27] The intramolecular dynamics acting to reduce the Δ' and Δ'' splittings in these $N = 1$ hot band states are also seen to increase the IR absorbances of the hot band Q spikes over those of the parent cold bands. This is observed below for several other fundamentals. The Ne-induced frequency shift for ν_{34} (b_2) is $^1/_2(1255.3 + 1256.2) - 1254.5 = +1.3$ cm^{-1}, and the Ar-induced frequency shift is -1.7 cm^{-1}.

2. ν_9 (a_1) = 1212.59 cm^{-1}. The MO computed (harmonic) frequencies (Tables 1 and 2) suggest the ν_{35} (b_2) and ν_9 (a_1) nominal CH rocking fundamentals are adjacent ($\omega_{35} - \omega_9 = 9$ cm^{-1}) and very weak ($Abs_{35} = 3$ and $Abs_9 = 2$ km/mol). The profile near 1210 cm^{-1} shown in Figures 2A and 7 is attributed to these overlapping modes. The sharp Q spike doublet of ν_9 (a_1) shown in Figure 7A lies 4.16 cm^{-1} to the blue—rather than 9 cm^{-1} to the red—of ν_{35} (b_2). Its components, 1212.52 and 1212.66 cm^{-1} in Figure 7B, yield (Table 1) ν_9 (a_1) = 1212.59 cm^{-1}, $DS_9 = |\Delta_9 - \Delta_0| = 0.14$ cm^{-1}, and $\Delta_9 = 1.11$ or 0.83 cm^{-1} (a 14% difference from Δ_0). The values[26] ν_9 (a_1) = 1214.2 (Ne), 1213 (Ar), and 1210 cm^{-1} (CS_2) show that the effective PES topography of Tp(OH) in this state is sensitive to intermolecular interactions.[26] The basic PQR profile seen for ν_9 (a_1) in Figure 7A is mirrored by a clear PQR profile at 1231 cm^{-1} for ν_9 (a_1) of gaseous Tp(OD).[26]

3. ν_{35} (b_2) = 1208.43 cm^{-1}. As summarized in lines 1−12 of Table 3 and shown in Figure 7C, the weak ν_{35} (b_2) fundamental of Tp(OH) follows the same spectral pattern shown by ν_{34} (b_2): a primary type B (*Y*-polarized) profile overlying a weak type A structure with Q spikes and accompanying hot band Q branch spikes. Complicating the spectrum, the hot band tunneling doublets are resolved, and there is also a doublet for the cold ($N = 0$) combination band[27] ν_{14} (a_1) + ν_{16} (a_2) = 349.1 + 859.0 = 1208.1 cm^{-1}. The multiple gas-phase transitions reduce to a single weak peak at 1207.5 cm^{-1} for Tp(OH) isolated in Ne. Assigned as Q branch peaks of ν_{35} (b_2), the 1207.50 and 1209.36 cm^{-1} ($N = 0$) peaks yield, as listed in Table 2, ν_{35} (b_2) = 1208.43 cm^{-1}, $DS_{35} = \Delta_{35} + \Delta_0 = 1.86$ cm^{-1}, and $\Delta_{35} = 0.89$ cm^{-1} (damped from Δ_0 by 8%). The ν_{35} (b_2) frequencies for Tp(OH) are 1208.43 (gas), 1207.5 (Ne), 1209 (sh) (Ar),[61] and 1208 (sh) (N_2)[61] cm^{-1}. The ν_{35}[Tp(OD)] (b_2) fundamental, 1213.1 cm^{-1} in Ne, is accompanied by peaks[16,26] at 1207.7 and 1233.7 cm^{-1} and by ν_9[Tp(OD)] (a_1) at 1231.1 cm^{-1}. The 1207.7 and 1233.7 cm^{-1} peaks are given the assignments $\nu_8 + \nu_{19}$ (A_2) = 1103.3 + 109 = 1212 cm^{-1} and $\nu_{12} + \nu_{22}$ (B_1) = 675 + 555 = 1230 cm^{-1} [strongly red-shifted into the region by deuterium isotope shifts of the ν_8 (COD bend) and ν_{22} (COD torsion) fundamentals].

4. ν_{33} (b_2) = 1315.21 cm^{-1}. Figure 8 shows that the central origin region for ν_{33} (b_2) contains a complex array of sharp spikes spanning 3 cm^{-1}. Of these, the weak peaks at 1314.28 and 1316.14 cm^{-1} ($N = 0$) in Figure 8B are assigned as the type A (*Z*-polarized) Q spikes for ν_{33} (b_2) to yield (Table 2) ν_{33} (b_2) = 1315.21 cm^{-1}, $DS_{33} = \Delta_{33} + \Delta_0 = 1.86$ cm^{-1}, and $\Delta_{33} = 0.89$ cm^{-1}. Lines 13−18 in Table 3 show that most of the remaining peaks in Figure 8B are assigned as resolved hot band doublets similar to those for ν_{35} (b_2) in Figure 7C, that is, as $\nu_{33} + N\nu_{26} - N\nu_{26}$ ($N = 1-4$) and $\nu_{33} + \nu_{19} - \nu_{19}$ ($N = 1$). The Ne-induced blue shift of ν_{33} (b_2) is ν_{33} (Ne) − ν_{33} (gas) = 1317.8−1315.21 = + 2.6 cm^{-1}, with Ar- and CS_2-induced blue shifts of +4.1 and +0.8 cm^{-1}, respectively.

IR peaks with medium intensities are observed at 1305.6 and 1317.8 cm^{-1} for Tp(OH) isolated in a Ne matrix, at 1306.5 and 1319.3 cm^{-1} in an Ar matrix, and at 1301 and 1316 cm^{-1} in CS_2 solvent.[16,26] The 1305.6 cm^{-1} peak (Ne) correlates with weak structure in the gas-phase absorbance shown in Figure 8A, and binary and ternary overtone and combination states are calculated[26] to fall nearby. The ν_{33} (b_2) state is evidently coupled to one or more of these states through resonance interactions such as often occur in the vibrational spectrum of Tp.

D. Tunneling Doublings in the 1375−1700 cm^{-1} Region (Figure 2B,C). Seven fundamentals, complex blendings of the COH bending, CC stretching, CO stretching, and CH rocking internal coordinates, occur in the 1375−1700 cm^{-1} range. They occur in a background of increasingly dense rotation−contortion−vibration states providing increasingly abundant

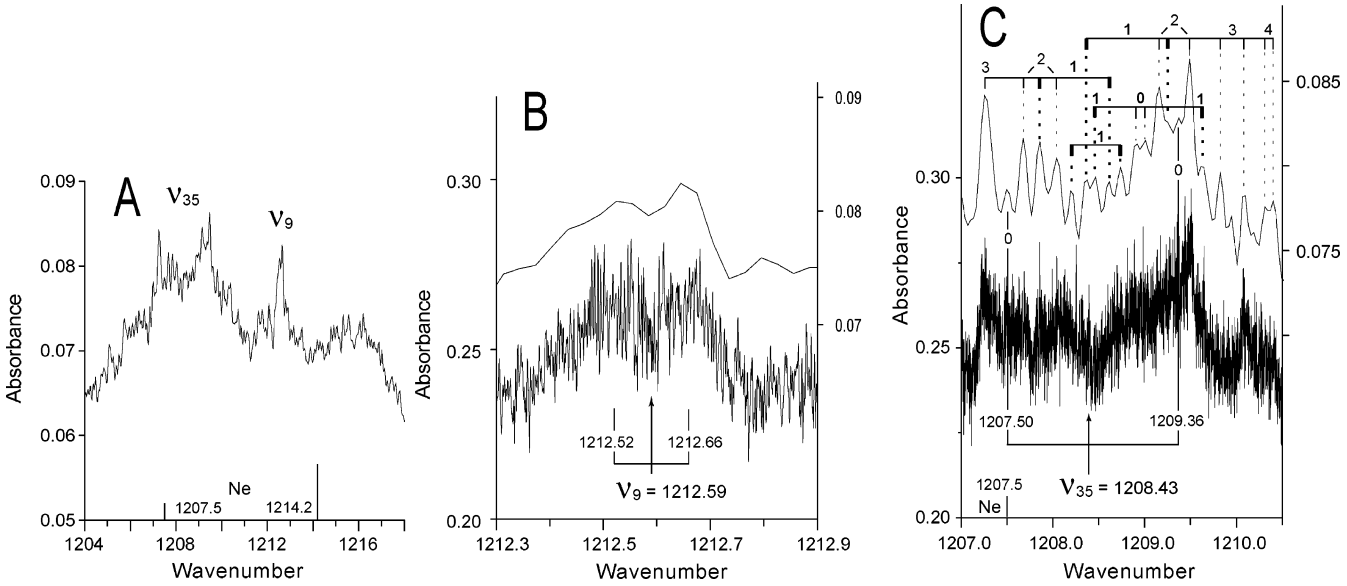

Figure 7. (A) IR absorption profile of the overlapping ν_{35} (b_2) and ν_9 (a_1) fundamentals shown at 0.10 cm^{-1} resolution. (B) Type A (*Z*-polarized) Q branch spike tunneling doublet yielding the vibrational frequency ν_9 (a_1) = 1212.59 cm^{-1}. (C) Assignment of the weak type A (*Z*-polarized) Q branch spikes yielding ν_{35} (b_2) = 1208.43 cm^{-1}, with accompanying hot band doublet transitions listed in lines 1−12 of Table 3. $N = 0$ for cold bands and $N \geq 1$ for hot bands. The observed frequencies in Table 3 are from the spectrum at 0.10 cm^{-1} spectral resolution.

TABLE 3: Hot Band Assignments

line	N	doublet (cm^{-1})	ν_{avg} (cm^{-1})	DS_v	$\nu_N - \nu_{N-1}$
		$\nu_{35} + N\nu_{19} - N\nu_{19}$[a]			
1	0	1207.50, 1209.36	1208.43	1.86	
2	1	1207.85, 1208.60	1208.23	0.75	−0.20
3	2	1207.67, 1208.04	1207.86	0.37	−0.37
4	3	1207.26, 1207.26	1207.26	0.0	−0.60
		$\nu_{35} + N\nu_{26} - N\nu_{26}$[a]			
5	1	1208.35, 1209.24	1208.80	0.89	0.37
6	2	1209.15, 1209.48	1209.32	0.33	0.52
7	3	1209.81, 1210.07	1209.94	0.26	0.62
8	4	1210.31, 1210.39	1210.35	0.08	0.41
		$\nu_{35} + N(\nu_{19} + \nu_{26}) - N(\nu_{19} + \nu_{26})$[a]			
9	1	1208.20, 1208.73	1208.47	0.53	0.04
		$(\nu_{14} + \nu_{16}) + N\nu_{19} - N\nu_{19}$[a]			
10	0	1208.90, 1208.99	1208.95	0.09	
11	1	1208.45, 1208.45	1208.45	0.0	−0.50
		$(\nu_{14} + \nu_{16}) + N\nu_{26} - N\nu_{26}$[a]			
12	1	1209.61, 1209.61	1209.61	0.0	0.66
		$\nu_{33} + N\nu_{19} - N\nu_{19}$[b]			
13	0	1314.28, 1316.14	1315.21	1.86	
14	1	1314.54, 1315.28	1314.91	0.74	−0.30
		$\nu_{33} + N\nu_{26} - N\nu_{26}$[b]			
15	1	1315.09, 1315.43	1315.26	0.34	0.05
16	2	1315.77, 1315.88	1315.83	0.11	0.57
17	3	1316.45, 1316.60	1316.53	0.15	0.70
18	4	1317.17, 1317.27	1317.22	0.10	0.69

[a] Figure 7C. [b] Figure 8B.

opportunities for resonance and other types of anharmonic couplings. The Ne matrix isolation data[16,26] in Figure 2 show many intense cold band transitions accompany these higher frequency fundamentals. It is noteworthy that no fundamental vibrations contribute directly to the strong central absorbance feature in Figure 2B.[26]

1. ν_{32} (b_2) = 1411.94 cm^{-1}. Figures 2B and 9A show weak peaks attributable to ν_{32} (b_2) on the P wing of the ν_7 (a_1) absorption, with a single peak at 1413.6 cm^{-1} for Ne-isolated Tp(OH). The assignment for the ν_{32} (b_2) region shown in Figure 9A produces DS_{32} = 1412.86 − 1411.01 = $\Delta_{32} + \Delta_0$ = 1.85 cm^{-1}. Then, as listed in Table 2, ν_{32} (b_2) = 1411.94 cm^{-1} and Δ_{32} = 0.88 cm^{-1}—a damping of 9% relative to Δ_0. Ne matrix interaction blue shifts the ν_{32} frequency by +1.7 cm^{-1}. The $\nu_{32} + \nu_{19} - \nu_{19}$ hot band doublet, with average frequency = 1411.39 cm^{-1} and $DS_{hot} = \Delta' + \Delta'' = 0.39$ cm^{-1}, is offset to the red of ν_{32} by −0.55 cm^{-1}. The small DS_{hot} value indicates Δ' and Δ'' are strongly damped relative to Δ_{32} and Δ_0.

2. ν_7 (a_1) = 1431.27 cm^{-1}. Figure 2B shows the PQR profile of ν_7 (a_1). As seen in Figure 9B, the Q branch region has a basic doublet of doublet pattern falling between nearly equivalent Ne matrix peaks[26] at 1427.1 and 1432.3 cm^{-1}. The gas-phase data suggest a resonance interaction occurs between ν_7 (a_1) and the CH wagging overtone state $2\nu_{23}$ (A_1) at 2(715.72) = 1431.44 cm^{-1}. $DS_{23} \approx 0$ cm^{-1} for the Q spike[27] of ν_{23} (b_1) at 715.72 cm^{-1}. Taking $2\nu_{23}$ (A_1) as a fixed zero-order point in the scheme mapped out in Figure 9C yields the preresonant value ν_7 (a_1) = 1431.27 cm^{-1}, with 0.33 cm^{-1} shifts of the zero-order states. The magnitude of the resonance splitting is strongly dependent on intermolecular environment, being 1431.77 − 1430.94 = 0.83 cm^{-1} in the gas phase versus 1432.3 − 1427.1 = 5.2 cm^{-1} in Ne (Figure 9B). The Ne-induced red shift of the averaged frequencies is −1.7 cm^{-1}. The postresonant $DS_7 \leq$ 0.14 cm^{-1} and $DS_{2\nu_{23}}$ = 0.15 cm^{-1} values are very similar. Taking DS_7 = 0.14 cm^{-1} as an upper limit to $|\Delta_7 - \Delta_0|$ yields $\Delta_7 \leq 1.11$ or ≥ 0.83 cm^{-1}, values differing from Δ_0 by up to 14% as listed in Table 1. Figure 9B shows that, unlike most other transitions in the FTIR spectrum at 25 °C covered by Figure 2, there are instances of systematic P and R branch structure. Thus, the spacing of the most intense lines (with full widths at half-maximum about 0.003 cm^{-1}) is 0.072 cm^{-1} in the 1427.6 cm^{-1} vicinity.

3. ν_6 (a_1) = 1502.53 cm^{-1}. The most intense IR absorption in Figure 2B is due to ν_6 (a_1), which is overlapped by at least three overtone-combination bands and additional hot band transitions. A resonance interaction paralleling that noted above for ν_7 (a_1) and $2\nu_{23}$ (A_1) is found for ν_6 (a_1) and $2\nu_{22}$ (A_1). Figure 10A shows the Ne matrix effect on the resonance-split states, namely 1505.2 − 1498.8 = 6.4 cm^{-1} (Ne) and 1502.86 − 1502.53 = 0.33 cm^{-1} (gas). Figure 10B shows ν_6 (a_1) = 1502.53 cm^{-1} and $DS_6 \approx 0$ cm^{-1} (Table 1). Further, with 1503.35 and 1502.36 cm^{-1} assigned as the type A (*Z*-polarized)

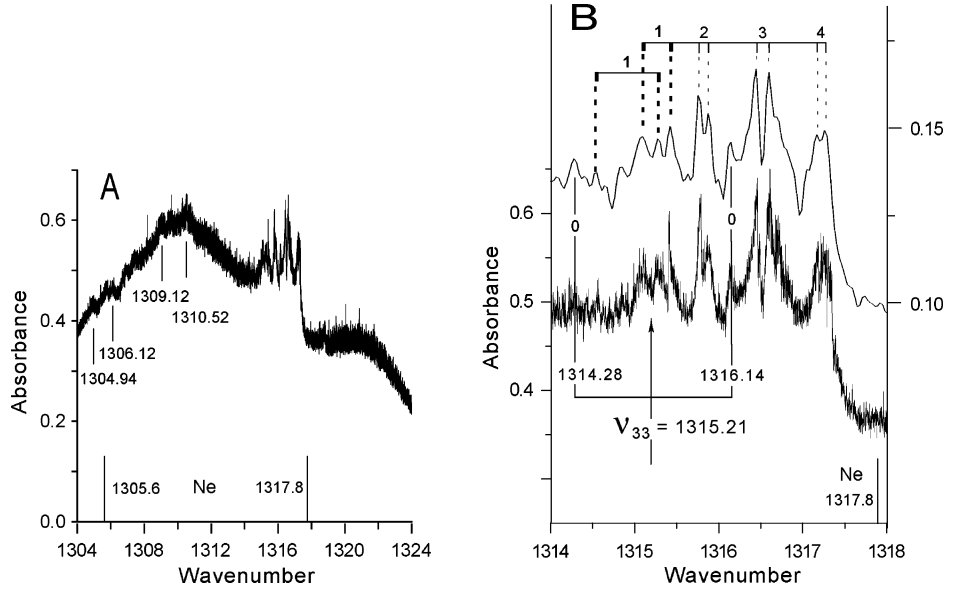

Figure 8. (A) FTIR spectrum for the ν_{33} (b_2) region at 0.0025 cm^{-1} resolution. (B) Assignment of weak type A (*Z*-polarized) Q branch spikes yielding ν_{33} (b_2) = 1315.21 cm^{-1}, with spectral detail and doublet assignments for hot band doublet progressions listed in lines 13−18 of Table 3.

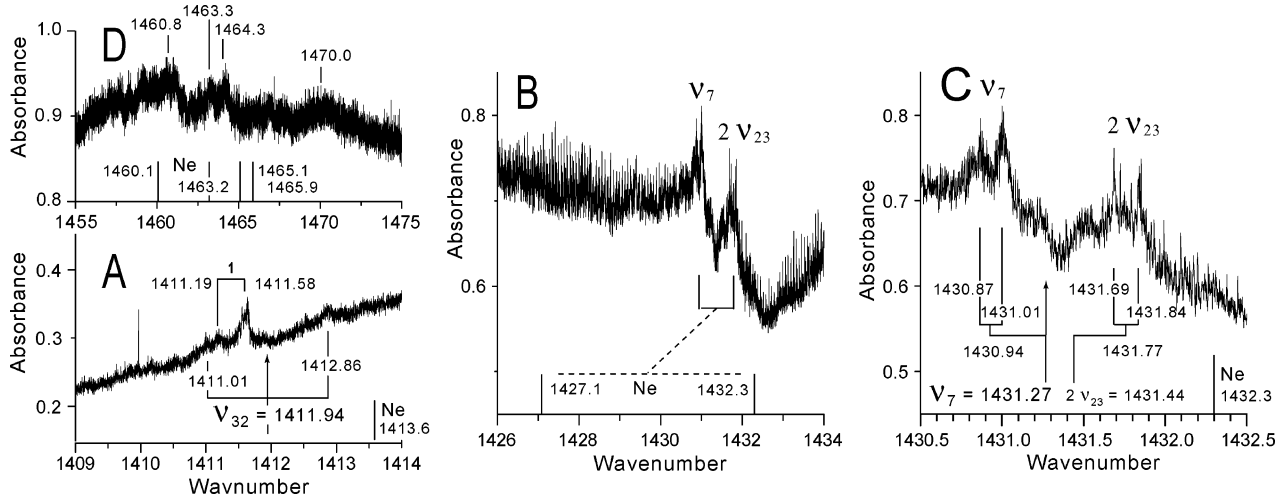

Figure 9. Details of FTIR absorbance profiles shown in Figure 2B. (A) Very weak type A (*Z*-polarized) Q branch spikes yielding ν_{32} (b_2) = 1411.94 cm^{-1}, with accompanying $\nu_{32} + \nu_{19} - \nu_{19}$ hot band doublet. (B) Central Q branch region showing resonance split ν_7 (a_1) and $2\nu_{23}$ (A_1) frequencies with the gas phase (0.83 cm^{-1}) and Ne matrix (5.2 cm^{-1}) separations. (C) Detail of the wide (resonance) and narrow (tunneling) doublings leading to the zero-order ν_7 (a_1) = 1431.27 cm^{-1} vibrational frequency. The $2\nu_{23}$ (A_1) = 1431.44 cm^{-1} value is an independent estimate.[27] (D) Overview of FTIR absorption in the 1455−1475 cm^{-1} crest region. None of the four cold band peaks is attributable to a fundamental vibration.

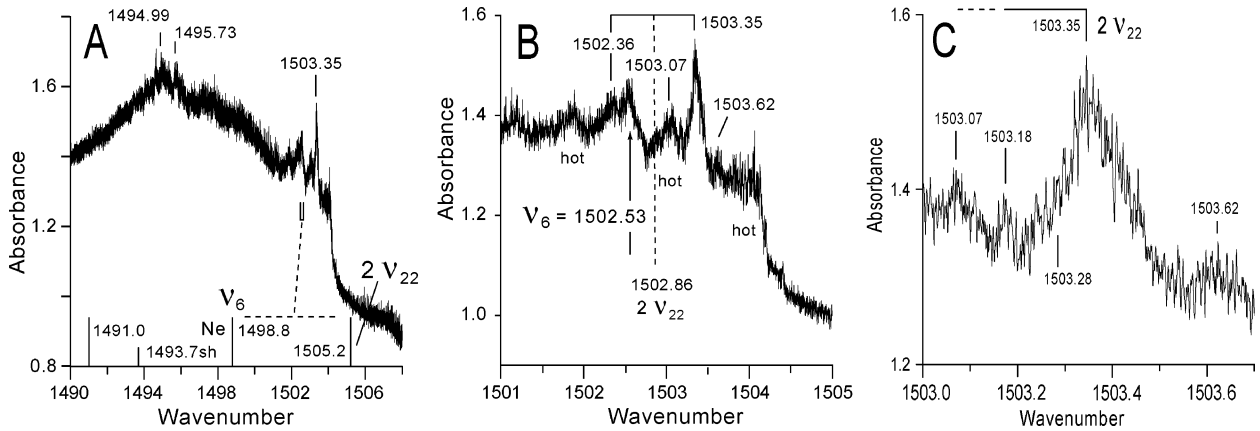

Figure 10. (A) Overview of IR absorption in the ν_6 (a_1) region showing resonance split ν_6 (a_1) and $2\nu_{22}$ (A_1) frequencies with the gas phase (0.33 cm^{-1}) and Ne matrix (6.4 cm^{-1}) separations. (B) Spectral detail of the Q spike region showing the ν_6 (a_1) = 1502.53 and $2\nu_{22} = {}^1/_2$(1502.36 + 1503.35) = 1502.86 cm^{-1} vibration frequencies. The zero-order $2\nu_{22}°$ value[27] is 1503.14 cm^{-1}, a position indicating higher than two-dimensional resonance interaction. Hot band transitions involving ν_{19} and ν_{26} are marked. (C) Spectral detail surrounding the 1503.35 cm^{-1} component of the $2\nu_{22}$ (A_1) type A (*Z*-polarized) Q branch doublet.

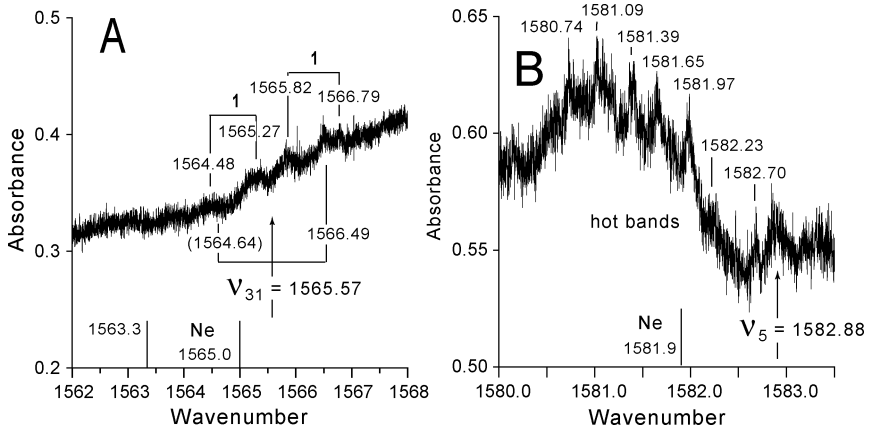

Figure 11. (A) Very weak type A (*Z*-polarized) Q branch spikes of ν_{31} (b_2) and adjacent hot band ($N = 1$) Q spikes. Although only one of the fundamental spikes is distinct, the FTIR data are consistent with the estimate ν_{31} (b_2) = 1565.57 cm^{-1} for the vibrational frequency. (B) Unresolved type A (*Z*-polarized) Q spike doublet for the ν_5 (a_1) = 1582.88 cm^{-1} vibrational frequency with unresolved doublet spikes for the adjacent hot band progression $\nu_5 + N\nu_{19} - N\nu_{19}$.

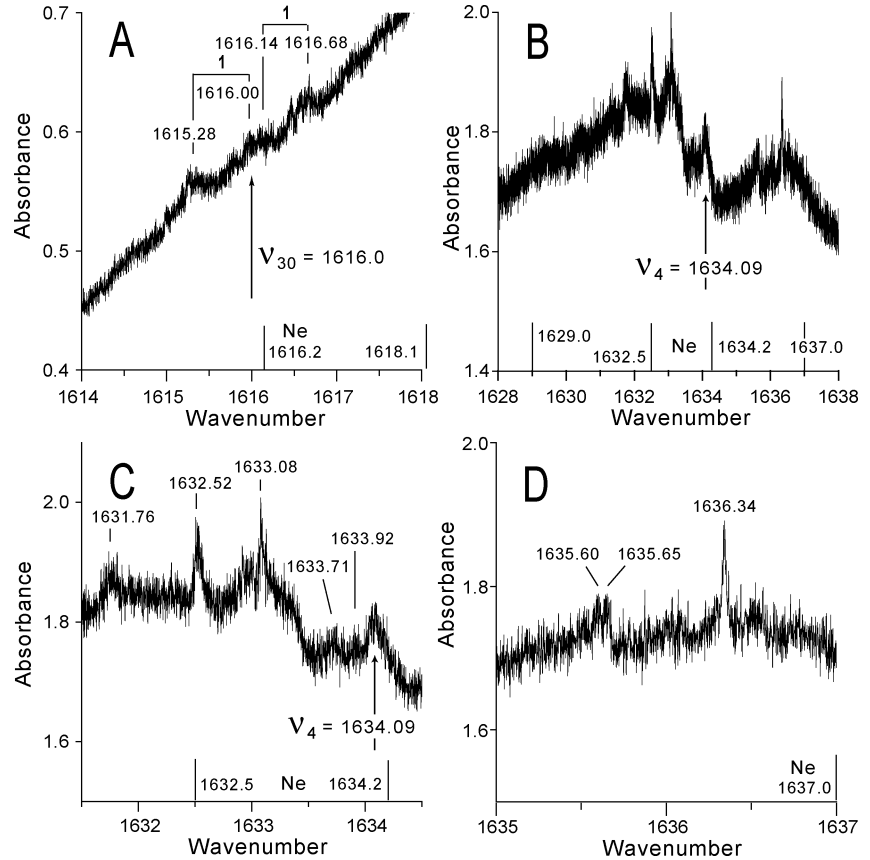

Figure 12. (A) Very weak type A (*Z*-polarized) Q branch spikes for the hot bands accompanying ν_{30} (b_2). The weaker spikes for ν_{30} (b_2) itself are not observed. (B) Overview of the complex absorption crest vicinity showing the basic PQR profile for the ν_4 (a_1) = 1634.09 cm^{-1} fundamental. (C) Unassigned peaks to the red of the unresolved Q branch doublet for ν_4 (a_1). (D) Unassigned peaks to the blue of the unresolved Q branch doublet for ν_4 (a_1).

tunneling doublet for $2\nu_{22}$ (A_1), $DS_{2\nu_{22}} = 0.99$ cm^{-1}. $\Delta_{22} = 0.07\Delta_0$ was reported[27] for the COH torsion to plausibly suggest $\Delta_{2\nu_{22}} \approx 0$ cm^{-1} and infer $DS_{2\nu_{22}} = |\Delta_{2\nu_{22}} - \Delta_0| \approx \Delta_0 = 0.974$ cm^{-1} predicted and 0.99 cm^{-1} observed. The resonance interaction seems likely to include states beyond ν_6 and $2\nu_{22}$. The absorptions marked as hot bands follow the patterns observed in previous figures. Figure 10C shows detail of the high-frequency Q spike entering $DS_{2\nu_{22}}$ (A_1). From the observed nominal frequencies, the Ne-induced vibrational frequency shift is $1498.8 - 1502.5 = -3.7$ cm^{-1}; from averaged frequencies for fully coupled ν_6 and $2\nu_{22}$ states, it is $^1/_2(1498.8 + 1505.2) - {}^1/_2[1502.53 + {}^1/_2(1502.36 + 1503.35)] = -0.7$ cm^{-1}.

4. ν_{31} (b_2) = 1565.57 cm^{-1}. Figures 2C and 11A show weak observed peak structure with the proposed assignments to ν_{31} (b_2) and accompanying hot bands $\nu_{31} + \nu_{19} - \nu_{19}$ (DS = 0.79 cm^{-1}) and $\nu_{31} + \nu_{26} - \nu_{26}$ (DS = 0.97 cm^{-1}). Then, as listed in Table 2, ν_{31} (b_2) = 1565.57 cm^{-1}, $DS_{31} = 1.85$ cm^{-1}, and $\Delta_{31} = 0.88$ cm^{-1}.

5. ν_5 (a_1) = 1582.88 cm^{-1}. Figures 2C and 11B show the 1582.88 cm^{-1} peak is assigned as the unresolved tunneling doublet for ν_5 (a_1), with an unassigned series of unresolved hot band tunneling doublets $\nu_5 + N\nu_{19} - N\nu_{19}$ leading to the red. Then $DS_5 \approx 0$ and $\Delta_5 \approx \Delta_0$ as listed in Table 1, and the Ne-induced vibrational red shift is $1581.9 - 1582.9 = -1.0$ cm^{-1}.

6. ν_{30} (b_2) = 1616.0 cm^{-1}. Figures 2C and 12A show resolved structure assignable as the hot band ($N = 1$) doublets $\nu_{30} + \nu_{19} - \nu_{19}$ (1615.28, 1616.00, DS = 0.72 cm^{-1}) and $\nu_{30} + \nu_{26} - \nu_{26}$ (1616.14, 1616.68, DS = 0.54 cm^{-1}) but showing no Q spikes attributable to ν_{30} (b_2). The rough estimate ν_{30} (b_2) = 1616.0 cm^{-1} (Table 2) is based on the observed hot bands and Ne matrix peaks.

7. ν_4 (a_1) = 1634.09 cm^{-1}. Figures 2C and 12B−D show the overview and details of the complex gas phase and Ne matrix spectra in the ν_4 (a_1) region. The ν_4 (a_1) [and ν_{30} (b_2)] fundamentals are both likely to be anharmonically coupled to some extent to other states by resonant and nonresonant interactions.[26] The relatively modest spike at 1634.09 cm^{-1} centers the apparent PQR profile seen in Figure 12B, and it is chosen as the unresolved Q spike doublet for ν_4 (a_1). It is shown with nearby peaks to the red in Figure 12C. Its profile and width show $DS_4 = |\Delta_4 - \Delta_0| \approx 0$ cm^{-1}, and $\Delta_4 \approx \Delta_0$, (Table 1). Figure 12D shows sharp peaks to the blue of ν_4 (a_1).

III. Concluding Discussion

A. Incipient IVR Processes and Δ_ν Values. The FTIR spectrum of Tp(OH) vapor contains sharp Q branch spikes yielding estimates for the separations DS_ν of spectral tunneling doublet components for 11 of the 12 fundamentals in the 1175−1700 cm^{-1} region. The overlapping rotational structures defy refined spectral analysis, but estimates for the Δ_ν values can be made from $DS_\nu = \Delta_\nu + \Delta_0$ (b_2 modes), $DS_\nu = |\Delta_\nu - \Delta_0|$ (a_1 modes), and the known value[24] $\Delta_0 = 0.974$ cm^{-1}. The highest three of the six a_1 fundamentals (Table 1) yield $\Delta_\nu \approx \Delta_0$ to suggest that tautomerization in the ν_4, ν_5, ν_6, and ZP states occurs on nearly identical effective PES topographies. Columns 5 of Tables 1 and 2 show the other eight Δ_ν values differ from Δ_0 by 5−14%. Therefore, none of the 11 effective PEF topographies is far removed from that in the ZP state—including ν_8 (a_1), the COH bending state. In contrast to these midrange Δ_ν values, $\Delta_{22} = 0.07\ \Delta_0$ (93% damping) for the COH torsion[27] [ν_{22} (b_1) = 751.57 cm^{-1}].

Uniformities shown by the observed midrange Δ_ν(Tp) values do not occur in calculations of the 21 Δ_ν(MA) values[32−35]—which are cited here as surrogate guides for the behavior to be expected from comprehensive computations for the full Δ_ν(Tp) set. The behavior observed for the midrange Δ_ν(Tp) splittings is reasonably attributable to the contributions of fast intramolecular vibrational energy redistribution (IVR) processes to the state-specific tunneling mechanisms. Current theories[66,67] address the IVR dynamics following the absorption of a photon into a bright molecular state coupled to a highly dense background of tiered dark states. Nonresonant and resonant anharmonic couplings are vital to the process, and direct evidence for these is ubiquitous in the observed vibrational spectrum of Tp. The observed Δ_ν(Tp) patterns invite the consideration of possible roles for the dense anharmonic dark background states to the tautomerization mechanism.

The absorption of a photon $h\nu_\nu$ by a tautomer in its ZP state results in a unique photoinduced change to the effective PES topography, which incorporates the vibrational energy. Fast intratautomer IVR processes delocalize and smooth this initial modification of the ZP PES into background states blanketing the entire molecule. With completed IVR the structured photoinduced component of the PES would be converted into a constant energy offset $h\nu_\nu$. At the limits of no IVR and completed fast IVR, the tunneling splittings are Δ_ν^ϕ and Δ_0, respectively. The observation that $\Delta_\nu \approx \Delta_0$ for three a_1 modes of Tp(OH) provides evidence for completed IVR processes in these states. The fast intratautomer and slower intertautomer (tunneling) IVR time scales may not be well separated for all steps. Under these conditions it is plausible that the observed splitting Δ_ν lies between the limits of Δ_ν^ϕ and Δ_0, that is, that $\Delta_\nu^\phi > \Delta_\nu > \Delta_0$ for states with dilated Δ_ν^ϕ, or $\Delta_\nu^\phi < \Delta_\nu < \Delta_0$ for states with damped Δ_ν^ϕ.

Damped excited-state tunneling, that is, $\Delta_\nu^\phi < \Delta_0$, is expected if tautomerization in the excited state includes the exchange of disproportionate atomic vibrational amplitudes between specific pairs of atoms. To illustrate, an exchange of the rather similar H(3) and H(7) displacements in Q_8 (a_1) (Figure 3) is facile and would minimally affect the tunneling splitting. However, exchange of the oppositely directed H(3) and H(7) displacements in Q_{34} (b_2) is not facile and this exchange must add dynamical complexity to the tunneling mechanism in the ν_{34} (b_2) state. As a minimum, it would contribute an increase to the effective tunneling path length, to produce a drive toward $\Delta_\nu^\phi < \Delta_0$. Since $\Delta_{34} = 1.05\Delta_0$ is observed, the various damping drives present in the ν_{34} (b_2) state do not prevail. However, with $\Delta_\nu \sim 0.90\ \Delta_0$ for ν_{35}, ν_{33}, ν_{32}, and ν_{31}, the damping drives for these states do prevail to produce $\Delta_\nu^\phi < \Delta_0$. Fast intratautomer IVR processes transform the four arguably quite different Δ_ν^ϕ values into similar Δ_ν values. Differing from Δ_0, the Δ_ν values indicate that PES bottlenecks have been reached, and that their topographies are relatively near that of the ZP state. The Δ_7, Δ_8, Δ_9, and Δ_{34} values in Tables 1 and 2 are sufficiently different from Δ_0 to suggest that the IVR processes acting on their Δ_ν^ϕ effective PES topographies have not completed before tunneling occurs. In contrast to the just-described behaviors, the low density of background dark states would inhibit IVR for ν_{22} (b_1), for which Δ_{22} is only $0.07\Delta_0$. The many strongly damped upper and lower states observed for the hot bands of Tp suggest (a) the effective PES of asymmetrically complex vibrational states tend inherently to produce a Δ_ν^ϕ value strongly damped relative to Δ_0, and (b) IVR processes of the effective PES tend to encounter bottlenecks limiting the degree of IVR modulation of Δ_ν^ϕ. The present status of experimental IVR measurements and of practical theoretical IVR computations is shown by the recent work on pyrrole and 1,3,5-triazine,[68] and on benzene.[69]

B. Tunneling Splittings in Malonaldehyde. The spectral behavior reported for Tp(OH) in this article is now compared with behavior observed in the midrange IR spectrum of MA.[7,10,13] The ZP tunneling splitting values are Δ_0[MA(OH)][8,9] = 21.583 cm^{-1} (which is $22.2\Delta_0$[Tp(OH)][24]) and the number of vibrational degrees of freedom exclusive of the OH/CH stretches is halved (17 for MA versus 33 for Tp). The much lower density of rotation−contortion−vibration background states for MA argues against the occurrence of IVR processes similar to those considered for the midrange fundamentals of Tp. Nevertheless, like Tp, the IR spectrum of MA(OH) shows evidence that $\Delta_\nu \approx \Delta_0$ for several of its midrange fundamentals.

Duan and Luckhaus[13] measured rotationally resolved transitions for the ν_6 (C═O/C═C stretch, COH bend) fundamental of jet-cooled MA(OH) at 1594 cm^{-1} using IR laser absorption spectroscopy and found $\Delta_6 - \Delta_0 = -0.03$ cm^{-1} (a 0.1% damping of Δ_6 relative to Δ_0). The ν_4[Tp(OH)] (a_1) fundamental at 1634.09 cm^{-1} with $\Delta_4 \approx \Delta_0$ is a close counterpart to ν_6[MA(OH)]. It occurs at a much higher background dark-state density than does ν_6[MA(OH)] and is apparently accompanied by more numerous close nonfundamental IR transitions. Grating studies of the IR spectrum of MA(OH) at spectral resolutions of 0.2−1 cm^{-1} show resolved apparent tunneling doublets for four of the lower frequency fundamentals.[7,10,13,70] Four additional transitions, all above 700 cm^{-1}, show sharp isolated spikes

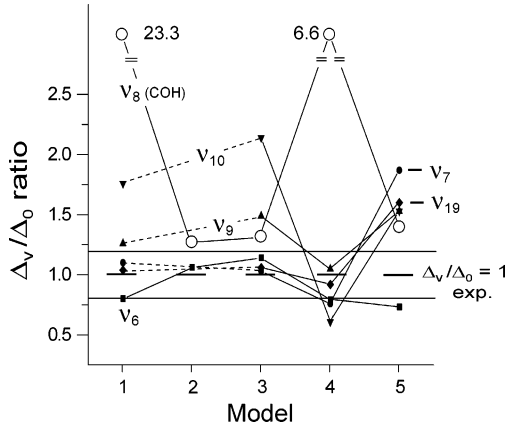

Figure 13. Ratios Δ_ν/Δ_0 of theoretically computed Δ_ν and Δ_0 values for six fundamentals of MA(OH) computed from theoretical models 1,[32] 2,[33] 3,[34] 4,[35] and 5.[35] The computed points are identified by use of vibrational assignments and observed frequencies listed in ref 71. Solid symbols refer to the points for ν_6 (1594), ν_7 (1452), ν_9 (1358), ν_{10} (1260), and ν_{19} (766 cm^{-1}), respectively, for which observed data suggest Δ_ν/Δ_0 is unity. Open circles refer to the points for ν_8 (1346 cm^{-1}), the nominal COH bending fundamental.[71] In very recent work,[73] however, the above-noted 1452 cm^{-1} spike, and a weaker one at 1435 cm^{-1}, are assigned as the resolved spectral tunneling doublet for the nominal COH bending fundamental.

reasonably expected to be unresolved tunneling doublets similar to those noted here for Tp(OH). According to the assignment listed by Alparone and Millefiori,[71] these latter four MA(OH) transitions are the in-plane fundamentals ν_7 (1452 cm^{-1}), ν_9 (1358 cm^{-1}), and ν_{10} (1260 cm^{-1}) and the out-of-plane fundamental ν_{19} (766 cm^{-1}). The vibrational assignments for MA are not confirmed,[7,10,13,70−72] and in very recent work-examining four state-specific tunneling doublets in gaseous MA(OH), Wassermann et al.[73] reassigned the above ν_7 (1452 cm^{-1}) transition. The 1451.7 spike and a weaker one at 1435.6 cm^{-1} are attributed to the tunneling doublet of the nominal COH bending fundamental to yield an upper state tunneling splitting estimate of 4−7 cm^{-1}, that is, a value strongly damped from Δ_0[MA(OH)] = 21.583 cm^{-1}.

The full set of 21 vibrational state-specific tunneling splittings Δ_ν(MA) has been addressed by four research groups using five different theoretical approximations.[32−35] With no consideration given the dark background states and fast IVR, $\Delta_\nu = \Delta_\nu^\phi$ for all the vibrational states of MA. In Figure 13 the solid symbols, stacked according to model number, present the Δ_ν/Δ_0 ratios computed for the five transitions noted above (ν_6, ν_7, ν_9, ν_{10}, and ν_{19}). (Points based on an obsolete vibrational assignment are omitted from the second column.) A strip highlighting computed values that fall in the 0.80−1.20 range contains 10 of the 21 filled points, and only the points for ν_{10} (the lowest frequency of the in-plane modes) fall exclusively outside the strip.

Given the similar IR data, normal coordinates, and Δ_ν values for ν_6[MA(OH)] and ν_4[Tp(OH)], it is reasonable to expect that the nominal COH bend transitions of MA(OH) and Tp(OH) also bear a resemblance. The nominal COH bending fundamental for MA(OH), according to the anharmonic computations of ref 71, is observed at ν_8 = 1346 cm^{-1}. This typically complex midrange fundamental has strongly mixed COH bend, CH rock, C═O stretch, and C═C stretch internal coordinates. The Δ_8/Δ_0 ratios computed[32−35] for this theoretical fundamental composition, which emphasizes dynamics of the transfer H, are shown as open circles in Figure 13. These computations would favor an analogous strong dilation of Δ_8^ϕ[Tp(OH)] relative to Δ_0[Tp(OH)], so that 1.07 cm^{-1} rather than 0.87 cm^{-1} (Table 1) would be chosen as the observed value of Δ_8[Tp(OH)] resulting from the modulation of Δ_8^ϕ by fast IVR. On the other hand, the reassignment of the nominal COH bending fundamental to the 1451.7, 1435.6 cm^{-1} doublet with its strongly damped Δ_{COH}(MA) value[73] would suggest that Δ_8^ϕ[Tp(OH)] is similarly strongly damped from Δ_0[Tp(OH)]. The fast IVR process would then modulate the PES topography to produce Δ_8[Tp(OH)] = 0.87 cm^{-1} as the observed value of choice.

Acknowledgment. The high-resolution FTIR data reported in this paper were recorded at the W. R. Wiley Environmental Molecular Sciences Laboratory, a national scientific user facility sponsored by the Department of Energy's Office of Biological and Environmental Research and located at Pacific Northwest National Laboratory. Pacific Northwest National Laboratory is operated for the U.S. Department of Energy by Battelle under Contract DE-AC06-76RLO1830. We thank Professor Suhm for sending us a copy of ref 73.

References and Notes

(1) Razavy, M. *Quantum Theory of Tunneling*; World Scientific Publishing Co. Pte. Ltd.: Singapore, 2003.
(2) Zuev, P. S.; Sheridan, R. S.; Albu, T. V.; Truhlar, D. G.; Hrovat, D. A.; Borden, W. T. *Science* **2003**, *299*, 867.
(3) Rowe Jr., W. F.; Duerst, R. W.; Wilson, E. B. *J. Am. Chem. Soc.* **1976**, *98*, 4021.
(4) Baughcum, S. L.; Duerst, R. W.; Rowe, W. F.; Smith, Z.; Wilson, E. B. *J. Am Chem. Soc.* **1981**, *103*, 6296.
(5) Turner, P.; Baughcum, S. L.; Coy, S. L.; Smith, Z. *J. Am. Chem. Soc.* **1984**, *106*, 2265.
(6) Baughcum, S. L.; Smith, Z.; Wilson, E. B.; Duerst, R. W. *J. Am. Chem. Soc.* **1984**, *106*, 2260.
(7) Seliskar, C. J.; Hoffman, R. E. *J. Mol. Spectrosc.* **1981**, *88*, 30.
(8) Firth, D. W.; Beyer, K.; Dvorak, M. A.; Reeve, S. W.; Grushow, A.; Leopold, K. R. *J. Chem. Phys.* **1991**, *94*, 1812.
(9) Baba, T.; Tanaka, T.; Morino, I.; Yamada, K. M. T.; Tanaka, K. *J. Chem. Phys.* **1999**, *110*, 4131.
(10) Smith, Z.; Wilson, E. B.; Duerst, R. W. *Spectrochim. Acta A* **1983**, *39*, 1117.
(11) Seliskar, C. J.; Hoffman, R. E. *J. Mol. Spectrosc.* **1982**, *96*, 146.
(12) Arias, A. A.; Wasserman, T. A. W.; Vaccaro, P. H. *J. Chem. Phys.* **1997**, *107*, 5617.
(13) Duan, C.; Luckhaus, D. *Chem. Phys. Lett.* **2004**, *391*, 129.
(14) Alves, A. C. P.; Hollas, J. M. *Mol. Phys.* **1972**, *23*, 927.
(15) Alves, A. C. P.; Hollas, J. M. *Mol. Phys.* **1973**, *25*, 1305.
(16) Redington, R. L.; Redington, T. E. *J. Mol. Spectrosc.* **1979**, *78*, 229.
(17) Rossetti, R.; Brus, L. E. *J. Chem. Phys.* **1980**, *73*, 1546.
(18) Tomioka, Y.; Ito, M.; Mikami, N. *J. Phys. Chem.* **1983**, *87*, 4401.
(19) Alves, A. C. P.; Hollas, J. M.; Musa, H.; Ridley, T. *J. Mol. Spectrosc.* **1985**, *109*, 99.
(20) Redington, R. L.; Chen, Y.; Scherer, G. J.; Field, R. W. *J.. Chem. Phys.* **1988**, *88*, 627.
(21) Redington, R. L.; Field, R. W. *Spectrochim. Acta A* **1989**, *45*, 41.
(22) Sekiya, H.; Nagashima, Y.; Nishimura, Y. *Bull. Chem. Soc. Jpn.* **1989**, *62*, 3229.
(23) Sekiya, H.; Nagashima, Y.; Nishimura, Y. *J. Chem. Phys.* **1990**, *92*, 5761.
(24) Tanaka, K.; Honjo, H.; Tanaka, T.; Kohguchi, H.; Ohshima, Y.; Endo, Y. *J. Chem. Phys.* **1999**, *110*, 1969.
(25) Frost, R. K.; Hagemeister, F. C.; Arrington, C. A.; Zwier, T. S.; Jordan, K. D. *J. Chem. Phys.* **1996**, *105*, 2595.
(26) Redington, R. L.; Redington, T. E.; Montgomery, J. M. *J. Chem. Phys.* **2000**, *113*, 2304.
(27) Redington, R. L.; Sams, R. L. *J. Phys. Chem. A* **2002**, *106*, 7494.
(28) Redington, R. L.; Sams, R. L. *Chem. Phys.* **2002**, *283*, 135.
(29) Bracamonte, A. E.; Vaccaro, P. H. *J. Chem. Phys.* **2003**, *119*, 997.
(30) Bracamonte, A. E.; Vaccaro, P. H. *J. Chem. Phys.* **2004**, *120*, 4638.
(31) Redington, R. L.; Redington, T. E.; Blake, T. A.; Sams, R. L.; Johnson, T. J. *J. Chem. Phys.* **2005**, *122*, 224311.
(32) Benderskii, V. A.; Vetoshkin, E. V.; Irgibaeva, I. S.; Trommsdorff, H. P. *Chem. Phys.* **2000**, *262*, 393.
(33) Sewell, T. D.; Guo, Y.; Thompson, D. L. *J. Chem. Phys.* **1995**, *103*, 8557.
(34) Meyer, R.; Ha, T.-K *Mol. Phys.* **2003**, *101*, 3263.
(35) Tew, D. P.; Handy, N. C.; Carter, S. *Mol. Phys.* **2004**, *102*, 2217.
(36) Carrington, T.; Miller, W. H. *J. Phys. Chem.* **1986**, *84*, 4364.

(37) Shida, N.; Barbara, P. F.; Almlöf, J. E. *J. Chem. Phys.* **1981**, *91*, 4061.
(38) Yagi, K.; Mil'nikov, G. V.; Taketsugu, T.; Hirao, K.; Nakamura, H. *Chem. Phys. Lett.* **2004**, *397*, 435.
(39) Smedarchina, Z.; Siebrand, W.; Zgierski, M. Z. *J. Chem. Phys.* **1995**, *103*, 5326.
(40) Giese, K.; Kühn, O. *J. Chem. Phys.* **2004**, *120*, 4107.
(41) Došlić, N.; Kühn, O. *Z. Phys. Chem.* **2003**, *217*, 1507.
(42) Tautermann, C. S.; Voegele, A. F.; Loerting, T.; Liedl, K. R. *J. Chem. Phys.* **2002**, *117*, 1962.
(43) Barone, V.; Adamo, C. *J. Chem. Phys.* **1996**, *105*, 11007.
(44) Sadhukhan, S.; Muñoz, D.; Adamo, C.; Scuseria, G. E. *Chem. Phys. Lett.* **1999**, *306*, 83.
(45) Yagi, K.; Taketsugu, T.; Hirao, K. *J. Chem. Phys.* **2001**, *115*, 10647.
(46) Makri, N.; Miller, W. H. *J. Chem. Phys.* **1989**, *91*, 4026.
(47) Coutinho-Neto, M. D.; Viel, A.; Manthe, U. *J. Chem. Phys.* **2004**, *121*, 9207.
(48) Mil'nikov, G. V.; Nakamura, H. *J. Chem. Phys.* **2001**, *115*, 6881.
(49) Mil'nikov, G. V.; Yagi, K.; Taketsugu, T.; Nakamura, H.; Hirao, K. *J. Chem. Phys.* **2004**, *120*, 5036.
(50) Tew, D. P.; Handy, N. C.; Carter, S.; Irle, S.; Bowman, J. *Mol. Phys.* **2003**, *101*, 2513.
(51) Vener, M. V.; Scheiner, S.; Sokolov, N. D. *J. Chem. Phys.* **1994**, *101*, 9755.
(52) Takada, S.; Nakamura, H. *J. Chem. Phys.* **1995**, *102*, 3977.
(53) Paz, J. J.; Moreno, M.; Lluch, J. M. *J. Chem. Phys.* **1995**, *103*, 353.
(54) Smedarchina, Z.; Siebrand, W.; Zgierski, M. Z. *J. Chem. Phys.* **1996**, *104*, 1203.
(55) Guo, Y.; Sewell, T. D.; Thompson, D. L. *J. Phys. Chem. A* **1998**, *102*, 5040.
(56) Wójcik, M. J.; Nakamura, H.; Iwata, S.; Wiktor, T. *J. Chem. Phys.* **2000**, *112*, 6322.
(57) Redington, R. L. *J. Chem. Phys.* **2000**, *113*, 2319.
(58) Tautermann, C. S.; Voegele, A. F.; Loerting, T.; Liedl, K. R. *J. Chem. Phys.* **2002**, *117*, 1967.
(59) Giese, K.; Kühn, O. *J. Chem. Phys.* **2005**, *123*, 054315.
(60) The GEN basis has 6-311G(df, pd) functions for the C−OH···O═C ring and 6-311G(d,p) functions for the C_5H_5 loop.[26,57]
(61) Rostkowska, H.; Lapinski, L.; Nowak, M. J.; Adamowicz, L. *Int. J. Quantum Chem.* **2002**, *90*, 1163.
(62) Bunker, P. R.; Jensen, P. *Molecular Symmetry and Spectroscopy*, 2nd ed.; NRC Research Press: Ottawa, Canada, 1998.
(63) Ueda, T.; Shimanouchi, T. *J. Mol. Spectrosc.* **1968**, *28*, 350.
(64) Redington, R. L.; Redington, T. E. *J. Chem. Phys.* **2005**, *122*, 124304.
(65) Except for the wide-spaced Δ_{27} (OH stretching) and Δ_{37} (skeletal contortion) values of the gaseous Tp(OH) and Tp(OD) isotopomers, the Δ_v values for fundamentals of Tp(OH) and Tp(OD) differ from $\Delta_0 = 0.974$ cm^{-1} by less than $\sim$1 cm^{-1} (ref 64). Gas-phase Δ_v values of $\sim$2 cm^{-1} or less are believed to be damped to near-zero by Ne matrix interactions to leave spectral "doublets", such as the 1272.3 and 1274.0 cm^{-1} Ne matrix peaks in Figure 5A, to be explained through multiple trapping sites or, when justified, special behaviors such as resonance coupled transitions.
(66) Lehmann, K. K.; Scoles, G.; Pate, B. H. *Annu. Rev. Phys. Chem.* **1994**, *45*, 241.
(67) Keske, J. C.; Pate, B. H. *Annu. Rev. Phys. Chem.* **2000**, *51*, 323.
(68) Callegari, A.; Pearman, R.; Choi, S.; Engels, P.; Srivastava, H.; Gruebele, M.; Lehmann, K. K.; Scoles, G. *Mol. Phys.* **2003**, *101*, 551.
(69) Callegari, A.; Merker, U.; Engels, P.; Srivastava, H. K.; Lehmann, K. K.; Scoles, G. *J. Chem. Phys.* **2000**, *113*, 10583.
(70) Redington, R. L. In *Handbook of Hydrogen Transfer*; Wiley−VCH Verlag GmbH: Weinheim, Germany; in press.
(71) Alparone, A.; Millefiori, S. *Chem. Phys.* **2003**, *290*, 15.
(72) Tayyari, S. F.; Milani-Nejad, F. *Spectrochem. Acta A* **1998**, *54*, 255.
(73) Wassermann, T. N.; Luckhaus, D.; Coussan, S.; Suhm, M. A. *Phys. Chem. Chem. Phys.* **2006**, *8*, 2344.